ACS OMEGA

Article

http://pubs.acs.org/journal/acsodf

Novel Polyethylene Fibers of Very High Thermal Conductivity Enabled by Amorphous Restructuring

Bowen Zhu,[†] Jing Liu,[†] Tianyu Wang,[†] Meng Han,[†] Shah Valloppilly,[‡] Shen Xu,[*,§] and Xinwei Wang[*,†]

[†]Department of Mechanical Engineering, Iowa State University, Ames, Iowa 50011, United States

[‡]Nebraska Center for Materials and Nanoscience, University of Nebraska at Lincoln, Lincoln, Nebraska 68588, United States

[§]Automotive Engineering College, Shanghai University of Engineering Science, 333 Longteng Road, 201620 Shanghai, P. R. China

Supporting Information

ABSTRACT: High-thermal-conductivity polymers are very sought after for applications in various thermal management systems. Although improving crystallinity is a common way for increasing the thermal conductivity (k) of polymers, it has very limited capacity when the crystallinity is already high. In this work, by heat-stretching a highly crystalline microfiber, a significant k enhancement is observed. More interestingly, it coincides with a reduction in crystallinity. The sample is a Spectra S-900 ultrahigh-molecular-weight polyethylene (UHMW-PE) microfiber of 92% crystallinity and high degree of orientation. The optimum stretching condition is 131.5 °C, with a strain rate of 0.0129 s^{-1} to a low strain ratio (~6.6) followed by air quenching. The k enhancement is from 21 to 51 W/(m·K), the highest value for UHMW-PE microfibers reported to date. X-ray diffraction study finds that the crystallinity reduces to 83% after stretching, whereas the crystallite size and crystallite orientation are not changed. Cryogenic thermal characterization shows a reduced level of phonon-defect scattering near 30 K. Polarization Raman spectroscopy finds enhanced alignment of amorphous chains, which could be the main reason for the k enhancement. A possible relocation of amorphous phase is also discussed and indirectly supported by a bending test.

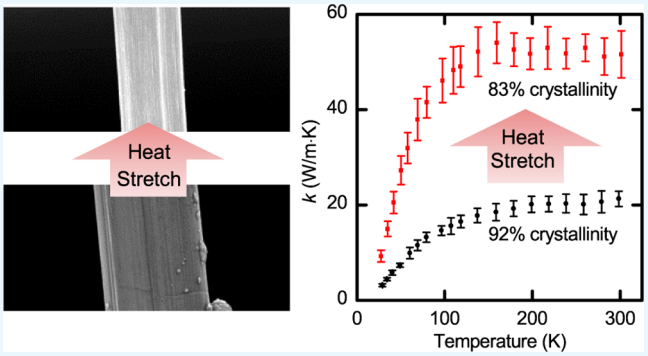

1. INTRODUCTION

Polymeric materials have been widely used in industry because of their low cost and excellent properties, including high strength-to-weight ratio, chemical stability, and corrosion resistance.[1−3] High thermal conductivity (k) can significantly improve polymers' capability of heat dissipation, tolerance to thermal impulse, and so on. Highly thermal conductive polymers are very sought after for applications in thermal design of flexible electronics as the substrate for excellent heat dissipation, apparel of reduced heat stress to quickly respread the accumulated heat from sensitive body areas, and to conduct the heat to the environment, and as fillers to make high-performance material interfaces used in central processing unit cooling. However, k of common synthetic polymers, including poly(ethylene terephthalate) (PET), low-density polyethylene (LD-PE), polypropylene, and poly(methyl methacrylate) (PMMA), universally falls in the range of 0.1−0.3 W/(m·K).[4−6] Attempts have been made to enhance k of polymers. Crystallinity and molecular orientation are two key factors that influence k. Usually, higher crystallinity leads to higher k due to the higher k of crystalline structures than amorphous structures. For example, the room-temperature (RT) k of an 81% crystalline PE is reported to be 70% higher than that of PE of 43% crystallinity.[5] Besides crystallinity, significant k enhancement is observed with improved molecular alignment, for both crystalline and amorphous polymers.[7−11] This is commonly understood that the covalent bonds along the polymer molecular chains sustain better energy transport than the van der Waals interaction between neighboring chains.[12] In practice, mechanical stretching is an effective way to enhance k. It has been observed that stretching improves molecular chain alignment and increases crystallinity. Piraux et al. improved the RT k of polyacetylene film up over 10 W/(m·K), with an approximate 500% elongation.[9] The molecular dynamic simulation of Liu et al. suggests that both k and degree of orientation increase with increased elongation for originally unoriented PE molecular cubes.[13] The work by Kurabayashi shows that the alignment of polymer chains could be correlated to anisotropic k of amorphous polymers like PMMA and polycarbonate.[11]

The heat-stretching process of PE for the production of highly thermal conductive fibers has been the subject of extensive research for several decades. Some high k values (9−104 W/(m·K)) have already been achieved in laboratory,[10,14−17] and k of defect-free PE chain predicted by simulation can be as high as 350 W/(m·K).[18] By ultra-drawing,

Received: June 12, 2017
Accepted: July 12, 2017
Published: July 26, 2017

DOI: 10.1021/acsomega.7b00563
ACS Omega 2017, 2, 3931−3944

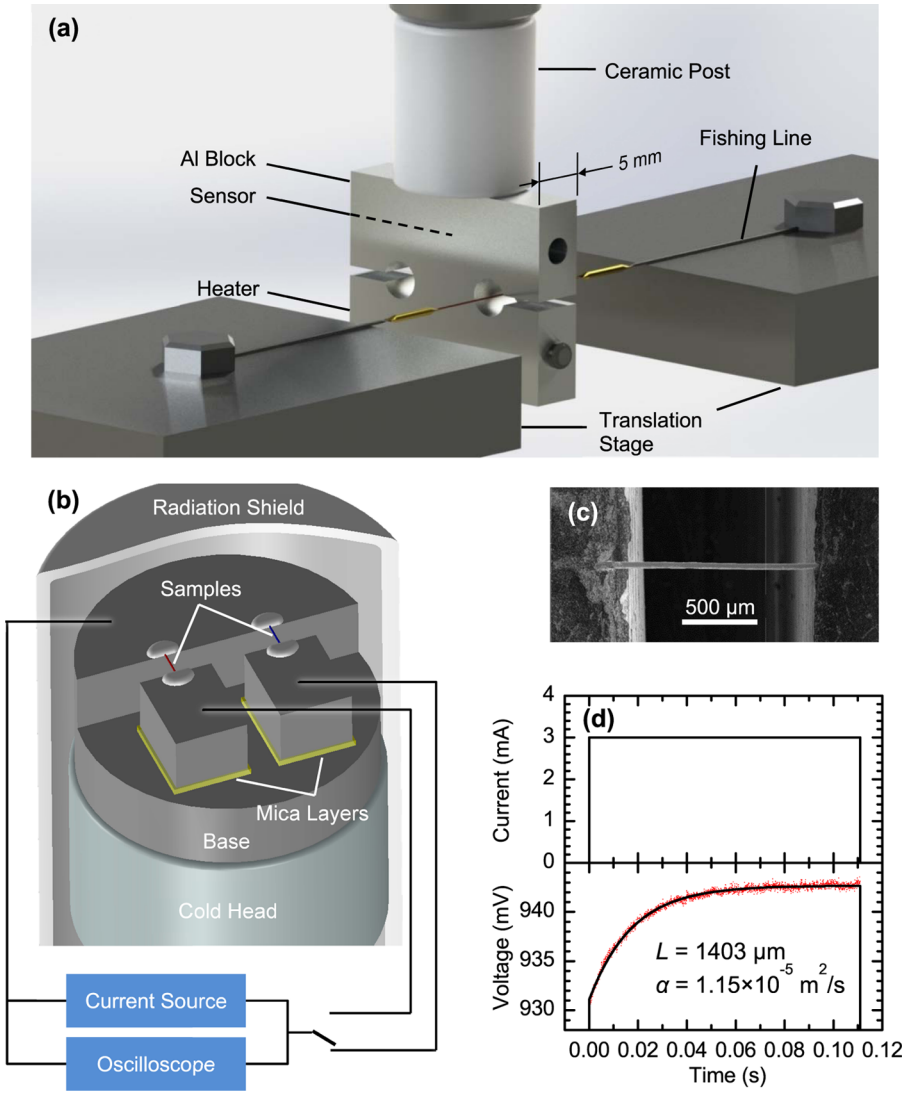

Figure 1. (a) Experimental setup of heat-stretching system. The Al block is integrated with a cartridge heater and a thermocouple sensor to provide a constant temperature during stretching. The temperature gradient along the sample fiber is estimated to be 10−40 K/mm, depending on center temperature. The center temperature of the sample fiber is measured by calibrating it to the sensor temperature (see Supporting Information). The two motorized translation stages move at a constant speed for each run. (b) Experimental setup for TET characterization. In a vacuum chamber (~0.5 mTorr) with radiation shield, the to-be-measured sample fibers are suspended between Al electrodes. Silver paste is employed to fix the samples onto electrodes. The electrodes are further connected to a direct current source and an oscilloscope. Thin mica layers provide electrical insulation. The Al base (the large electrode) is attached to the cold head by thermal grease. (c) Scanning electron microscopy (SEM) image of a sample prepared for TET characterization. The sample is unstretched sample C, which will be mentioned later. (d) Current input and voltage−time evolution for unstretched sample C at RT.

PE film's k has been increased from 6 to 41 W/(m·K) by Choy et al.[10] Their sample, ultrahigh-molecular-weight polyethylene (UHMW-PE) single-crystal mat, was produced using the method of Kanamoto et al.[19] and further stretched to a strain ratio of 350 with a strain rate of 0.083 s^{-1} at 125 °C. The final mat thickness is 8 μm. For thermal characterization, Choy et al. used the laser-flash radiometry technique[20] at 160−300 K and steady heat flow method below 160 K. The gel-spun UHMW-PE microfibers are measured to have $k \approx 60$ W/(m·K) (DSM Dyneema fiber) by Fujishiro et al.[14] using steady heat flow method and $k \approx 12-17$ W/(m·K) (DSM Dyneema fiber and Honeywell Spectra fiber) by Wang et al.[15] using time-domain thermoreflectance (TDTR) method. The measured k values in refs 10 and 14 could be overestimated because both groups employed conventional steady-state measurement method without subtracting the radiation effect. A considerable portion of the measured k could come from the contribution of heat radiation when the sample has a large length-to-diameter ratio (the ratio is over 50 in ref 14). The k of electrospun PE nanofibers was measured to be 9.3 W/(m·K) by Ma et al.[16] using the micromachined thermal bridge method.[21] The k of PE nanofiber, picked from UHMW-PE gel with a fine tungsten tip, was increased to an astonishing value as high as 104 W/(m·K) by further ultra-drawing, as reported by Shen et al.[17] Their sample was elongated to 131 nm in diameter and 290 μm in length with an estimated draw ratio of 60−800.[17] Their thermal characterization was carried out by utilizing a bimaterial cantilever as temperature sensor and a needle heater in high vacuum.

Recently, our group has done systematic research on the thermal properties of UHMW-PE fibers. Liu et al. conducted an in-depth study on the thermal properties of UHMW-PE

DOI: 10.1021/acsomega.7b00563
ACS Omega 2017, 2, 3931−3944

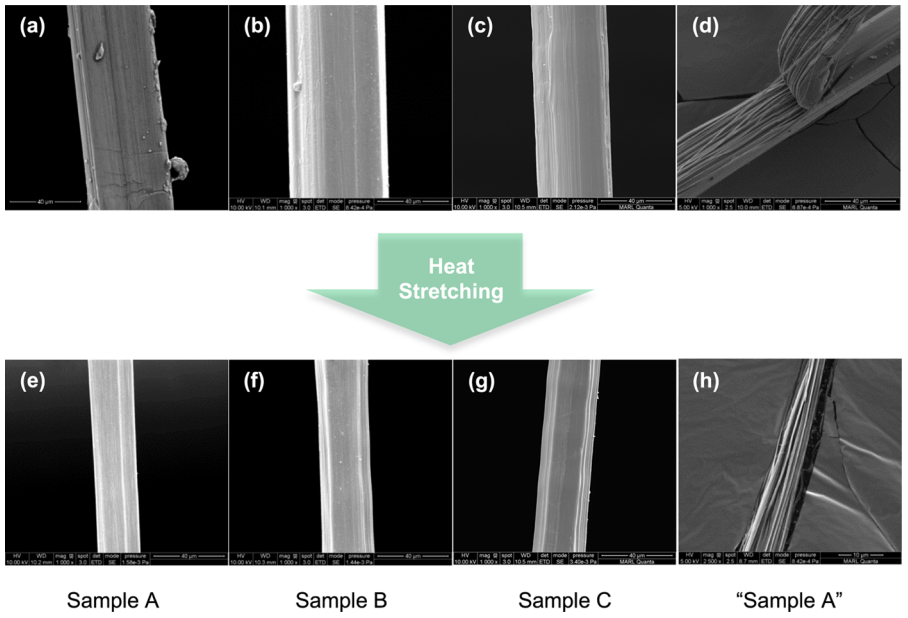

Figure 2. SEM images of UHMW-PE fibers before and after heat stretching: (a), (b), (c), and (d) represent reference samples for the stretched ones (e), (f), (g), and (h), respectively. (a, d) A fiber sample (sample A) stretched at a rate of 10 μm/s at 131.5 °C. (b, f) A fiber sample (sample B) stretched at a rate of 10 μm/s at 124.5 °C. (c, g) A fiber sample (sample C) stretched at a rate of 10 μm/s at 116 °C. (d, h) A duplicate of sample A split into two branches, with one branch facing upward, as shown in (h).

microfibers (Honeywell Spectra S-900) from RT to 10 K using the transient electrothermal (TET) technique.[22] Sample's k at RT is measured to be ~23 W/(m·K). The defect-induced phonon mean free path (MFP) is evaluated to be 8.06 and 9.42 nm for the two samples under study, relatively smaller than the axial crystallite size of 19.7 nm. This difference is attributed to extensive phonon scatterings at grain boundaries.

To date, no other studies have reported high k values comparable to those found by Choy et al. and Shen et al.[10,17] Also, their k improvement needs sample ultra-drawing. In this work, we aim to improve the k of microscale UHMW-PE fibers, which are applicable at the engineering level. By combining well-controlled and optimized heating and stretching of UHMW-PE crystalline fibers at a moderate level, we significantly improved the k to the level of 50 W/(m·K), maintaining the drawing ratio very low (~6.6). Three groups of samples stretched under different conditions were measured using the TET technique from RT to 30 K. To uncover the mechanism of this significant k improvement, a thermal reffusivity study of phonon MFP and a pole-figure X-ray diffraction (XRD) study were conducted. The result of XRD analysis indicates a decreased crystallinity although with a significant increase in k. The contradictory could be attributed to the reconstruction of amorphous region, including distribution and alignment. Further study by polarized Raman spectra indicates enhanced amorphous alignment after heat stretching.

2. RESULTS AND DISCUSSION

2.1. Effect of Heating Level and Stretching Speed. Honeywell Spectra S-900, a commercial UHMW-PE fiber of high tensile modulus (73 GPa) and high crystallinity (92%), was supplied by Minifibers, Inc. in the form of 50 mm cut. Sample thickness varies between 40 and 55 μm. The density is 0.97 g/cm^3. Each sample fiber is further cut into two parts: 40 mm, for heat stretching, and 10 mm, as reference.

Heat stretching is carried out by applying constant temperature and constant stretching speed to sample fibers, followed by quenching in air. The setup of the heat-stretching system is shown in Figure 1a. The idea of the setup has come from the optical fiber tapering method developed by Rudy and colleagues.[23] Then, we apply the TET technique to measure the thermal diffusivity, α, of stretched samples and reference samples at RT. The value of k is obtained as $k = \alpha\rho C_p$, where ρC_p is the volumetric heat capacity given by our previous work on S-900 fiber.[22] TET is a transient thermal characterization technique that utilizes electric current to generate and detect temperature change. The TET technique has been proven of sound accuracy (high signal-to-noise ratio) and reliability (no calibration required) for measuring α of a single microfiber in a wide temperature range (10−300 K).[22,24,25] It has great advantages over the other three thermal characterization techniques for microfibers: 3-omega, TDTR, and micro-fabricated thermal bridge method.[15,26,27] The setup for TET characterization is presented in Figure 1b−d. A more detailed description of the heat stretching and TET characterization is included in Supporting Information.

It should be mentioned that in the subsequent discussion on k, the error of ρC_p is not considered in error analysis. The value of ρC_p is evaluated using ρC_p of crystal PE and amorphous PE (obtained by extrapolation) from the literature.[28,29] Therefore, error of ρC_p is very hard to evaluate. The ρC_p used in this work is nevertheless reliable because (1) the ρC_p of crystal PE is well defined by both simulation and experiment,[28,29] (2) the sample used in this work is highly crystalline (83−92%), and (3) for amorphous PE and crystal PE, the difference in ρC_p is not significant (within 20% in the temperature range of 30−300 K).[29]

Heat stretching here covers a temperature range of 116−135 °C. The reason is that we cannot find significant elongation and k enhancement below 116 °C. Initially, heat stretching has been performed between RT and 90 °C in water bath. Low-temperature stretching leads to a k enhancement less than 4

DOI: 10.1021/acsomega.7b00563
ACS Omega 2017, 2, 3931−3944

Table 1. Stretching Conditions and Corresponding Results for Samples A–C

	samples		
	A	B	C
stretching velocity (μm/s)	10	10	20
stretching temperature (°C)	131.5	124.5	116.0
k increase at RT (W/(m·K))	20.7 → 51.8	20.5 → 40.5	18.9 → 34.4
diameter change (μm)	36.0 → 14.0	42.6 → 20.7	36.7 → 23
strain ratio	6.59	4.22	2.55
strain rate (s^{-1})	0.0129	0.0082	0.0155

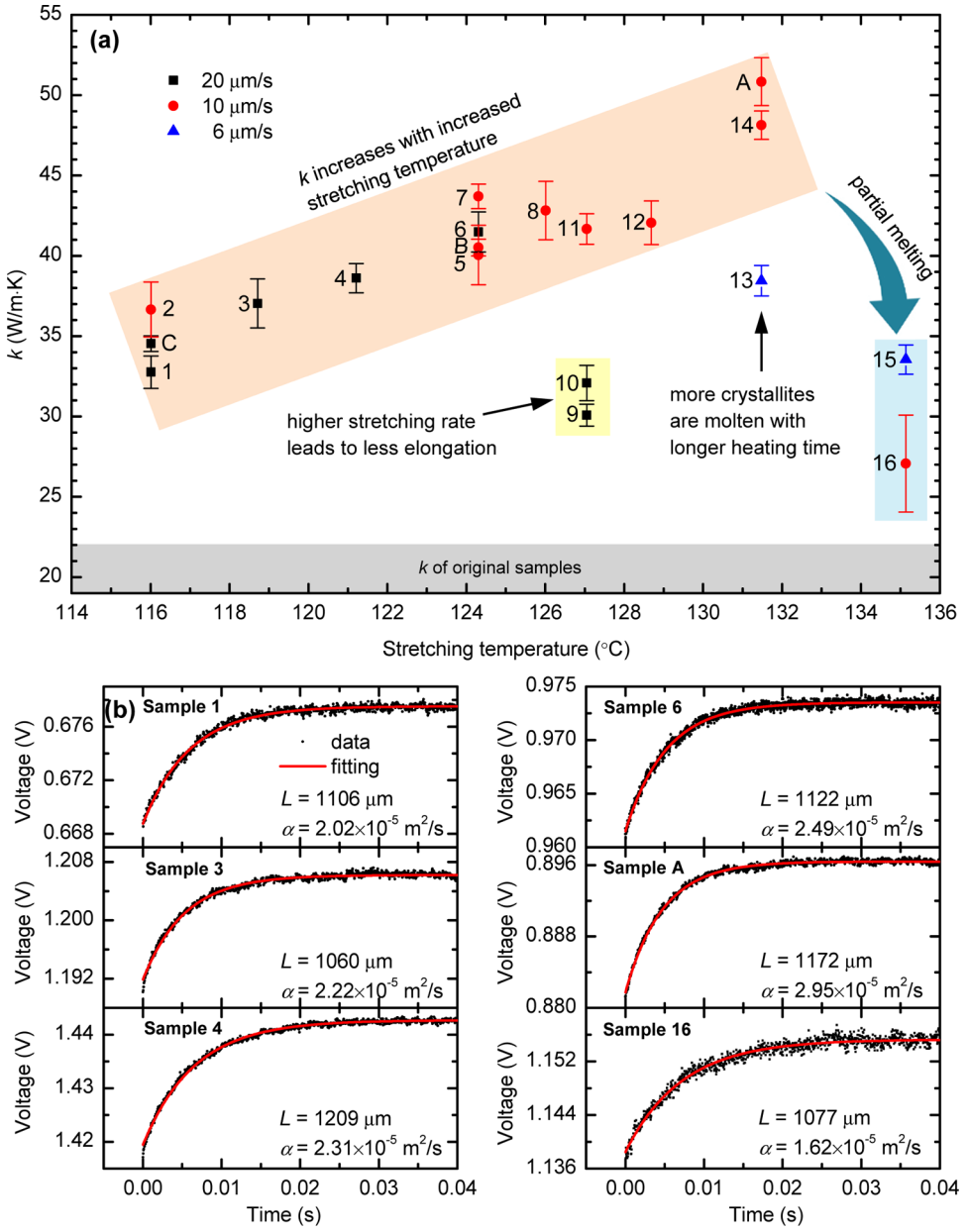

Figure 3. (a) RT k of UHMW-PE fibers after being stretched at different rates and different temperatures. Each data point is a mean value of 20 repeated measurements. The error bar represents three standard deviations of the mean. Besides samples A–C, other samples are denoted by numbers 1–16. The gray zone represents the measured k of original samples. (b) Representative raw data for samples stretched under different conditions, including samples 1, 3, 4, 6, A, and 16 in (a). It shows a sound signal-to-noise ratio and fitting agreement to give a highly reliable α.

W/(m·K), whereas k of original fibers can vary between 19 and 22 W/(m·K). Above 135 °C, a fiber breaks nearly without resistance to applied force. It seems the majority of fiber content has molten, although the suspended fiber nevertheless holds its shape before stretching, possibly due to the very long molecular chain. The stretching speed includes three values for comparison: 6, 10, and 20 μm/s. Stretching at over 20 μm/s limits the elongation and resultant k enhancement. The

DOI: 10.1021/acsomega.7b00563
ACS Omega 2017, 2, 3931–3944

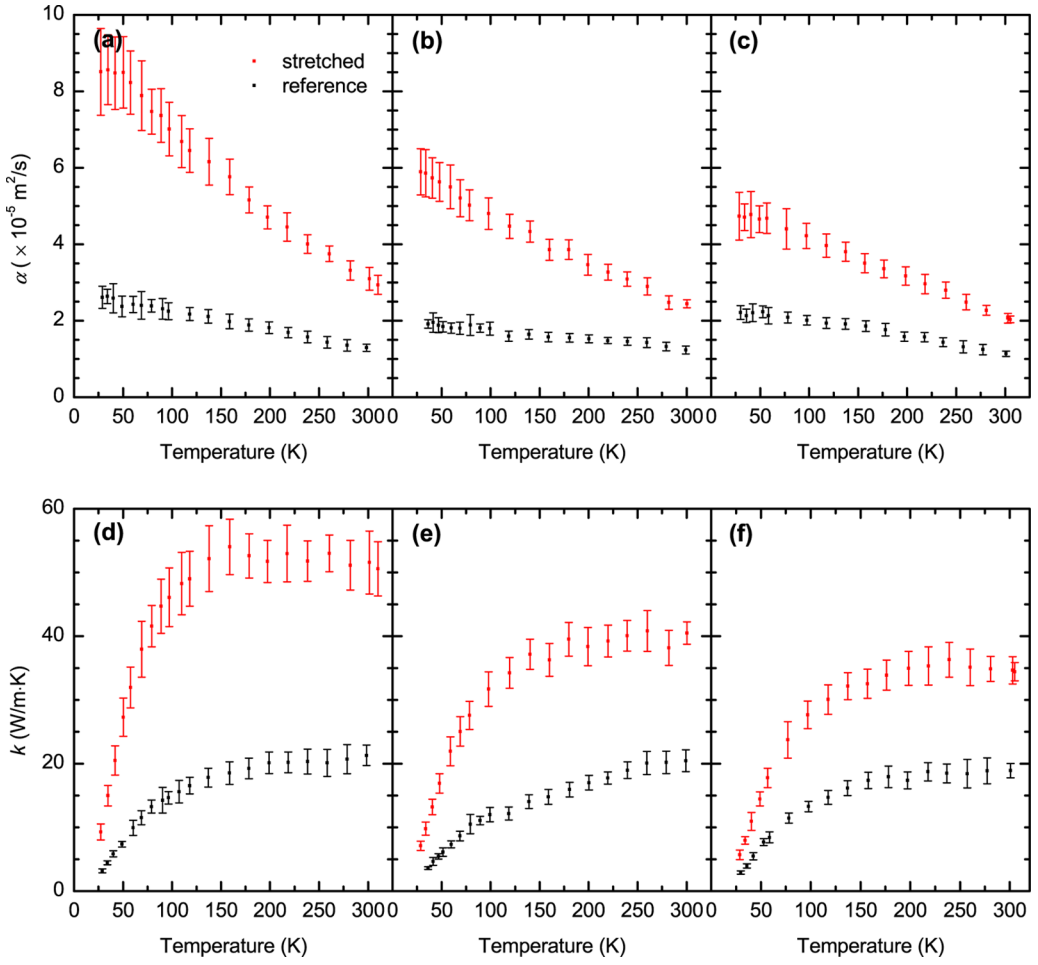

Figure 4. α and k vs temperature for samples A–C. (a), (b), and (c) α vs temperature for samples A, B, and C, respectively; (d), (e), and (f) the corresponding k against temperature. The error bar represents three standard deviations of the mean for 20 measurements at a temperature.

minimum speed given by the motorized translation stages is 6 μm/s. Therefore, the stretching conditions that are selected to present include 116–135 °C as the temperature range and 6–20 μm/s as the speed range. Under such conditions, the strain rate is estimated to be between 0.008 and 0.016 s^{-1} by measuring local fiber width.

During the stretching process, distinct necking appears with a large decrease in thickness of the fiber, as shown in Figure 2a–c,e–g. Beside the neck region is the shoulder region, which is heated at the beginning but then gets gradually drawn away from the heated region. The rest is stretched but not heated. The thickness of the unheated part is identical to that of the reference samples, which are neither heated nor stretched. The length of the neck region is 3–5 mm. The samples as presented are three typical scenarios (samples A–C) we study in this work. The stretching conditions of the three samples are summarized in Table 1. The internal structure is investigated by mechanical splitting. Figure 2d,h shows the axial cross section of a stretched sample and its reference sample, respectively. It can be seen that the original microfiber is composed of numerous finer fibers highly aligned in submicron scale, which somehow explains the high k (19–22 W/(m·K)) of S-900 fiber. After stretching under the same condition as sample A, the internal structure remains clearly stranded and aligned as well as that of original S-900.

For thermal characterization, we merely sample the center (3 mm long) of the fiber neck for stretched fibers. It is because every sample has been elongated by 3 mm at least. The change in k of samples stretched under different conditions is presented in Figure 3a, with the fitting quality of thermal characterization shown in Figure 3b. There is a clear trend that the value of k increases with increased stretching temperature, from 116 to 131.5 °C, as highlighted in the figure. This is due to the longer elongation by stretching (before break) when a higher temperature is used. At 131.5 °C, it reaches a peak. The optimal temperature (131.5 °C) is very close to 130 °C, where Smith et al. achieved a high degree of orientation for drawn UHMW-PE gel film (strain ratio = 130).[30] Over 131.5 °C, the heated fiber seems free from stress, but it still holds its shape probably due to the extremely long molecular chain of UHMW-PE. The elongation at break and k improvement are smaller than those at lower stretching temperature. For example, the sample (sample 16) stretched at 135 °C by 3.3 mm has a lower k (26.9 W/(m·K)) than sample A stretched at 131.5 °C by 5 mm. As the temperature exceeds 135 °C, the fiber melts before being stretched. The highest k value at RT obtained here is 50.8 W/(m·K) when a fiber is stretched at a rate of 10 μm/s at 131.5 °C (sample A). Figure 2a,e shows the fiber thickness before and after stretching. Sample A is of great interest and will be studied in detail in the following sections.

For the stretching rate effect, Figure 3a shows a weak dependence of k on the stretching rate. We use a relatively high stretching rate at low temperatures, 20 μm/s. When the temperature is higher than 124.5 °C, the faster stretching will

DOI: 10.1021/acsomega.7b00563
ACS Omega 2017, 2, 3931–3944

quickly break the sample, and is not suitable for the stretching. Therefore, a lower stretching rate of 10 μm/s is used. This can be clearly proved by the two stretching results at 127 °C. The two samples (samples 9 and 10) stretched at 20 μm/s at 127 °C have a much lower k than sample 11 stretched at 10 μm/s at the same temperature. The overall elongations of these two fibers are both 3 mm, which is considerably shorter than the 5 mm elongation of the fiber (sample 11) stretched at the same temperature with a half speed (10 μm/s). It suggests that a high stretching speed might limit the maximum elongation at a threshold temperature, leading to a less improved k value. As the lower limit, 6 μm/s is tried at 131.5 °C (sample 13). However, the k value drops significantly. A possible reason is that the lower stretching speed provides longer time for the PE to melt, which weakens the effect of stress.

The strain rate could be a key for the high k achieved in this study. It is because the internal tensile stress is related to the strain rate and a moderate level of internal tensile stress could align molecular chains without breaking them. The strain rate used in this work (0.008−0.016 s^{-1}; average, 0.0129 s^{-1}, for sample A) is close to the range of 0.01−0.1 s^{-1}, where optimal chain alignment, crystallinity, and elastic modulus were found for stretched UHMW-PE materials. Examples include 0.011, 0.033, and 0.083 s^{-1} for microfiber (a blend with 2 wt % LDPE), single-crystal mat, and single-crystal film, respectively.[10,31,32]

2.2. Thermal Conductivity Behavior under Measurement Temperature Variation. After RT thermal characterization, sample A stretched at 131.5 °C and other two fibers stretched at 124.5 °C (sample B) and 116 °C (sample C) are selected for further cryogenic TET measurement. These cryogenic studies are to provide further knowledge on how k and α of stretched PE fibers increase over those of unstretched ones. Also, a detailed study of the stretching ratio is conducted. Properties and elongation details of the samples are listed in Table 1. The fiber thickness has already been measured under SEM, as shown in Figure 2a−c,e−g.

The cryogenic TET test gives α and k at different temperatures from 30 to 300 K, as shown in Figure 4. The data of the stretched samples and reference samples are compared. k is calculated according to the reported ρC_p.[22] The figures show that, for the stretched and reference samples, α decreases monotonically with increased temperature whereas k does not. In the plots of k, a subtle decrease with increased temperature near RT could be observed. It is due to the combination effect of increasing ρC_p and decreasing α with increased temperature. The increase of ρC_p becomes moderate near RT, which allows $k = \alpha\rho C_p$ to follow the decrease of α. This phenomenon is also observed and studied in the literature.[4−6,33] By comparing the stretched and reference samples, it is observed that not only at RT but also at any temperature below RT, the stretched samples have much higher k and α. To rule out the effect of difference among unstretched fibers, we should introduce the k increase ratio, k_{str}/k_{ref}, which is the k of stretched sample divided by that of the reference sample. In Figure 5, k_{str}/k_{ref} is plotted against temperature. As temperature decreases to 30 K from RT, k_{str}/k_{ref} increases from 2.4 to 3.3 for sample A, from 1.5 to 2.8 for sample B, and from 1.8 to 2.5 for sample C, suggesting a more pronounced enhancement of k under cryogenic temperatures.

2.3. Low-Momentum Phonon MFP Improvement by Heat Stretching. The cryogenic TET characterization suggests that stretching UHMW-PE fibers at 10 μm/s at 131.5 °C leads to the most significant improvement of k and α in a wide temperature range. To unveil the mechanism behind the significant improvement of k, phonon MFP calculation and XRD and Raman spectroscopy analyses are employed.

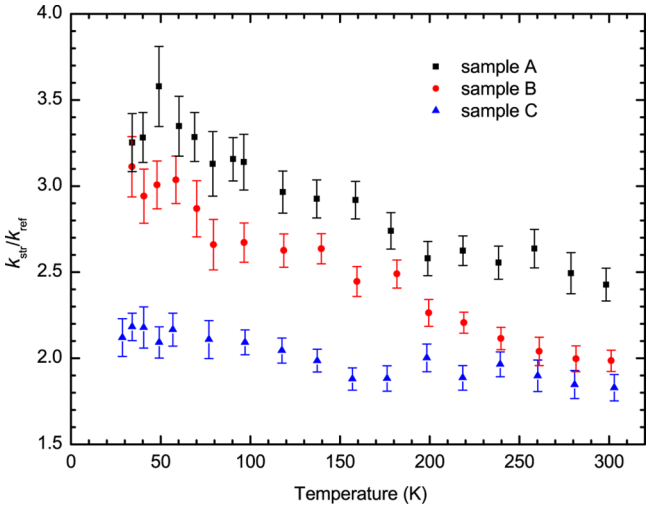

Figure 5. k improvement ratio k_{str}/k_{ref} against temperature for samples A−C. k_{str} and k_{ref} come from the experimental data of Figure 4. The error bar represents standard deviation of the mean.

The defect-induced phonon MFP can be evaluated by thermal reffusivity Θ, reciprocal of α, at the 0 K limit.[34] The idea is that a phonon is much more likely to be scattered by defects rather than other phonons at extremely low temperature because the majority of phonons are "frozen out". Under single-relaxation-time approximation, Θ can be expressed as $\Theta = 3v^{-1}l^{-1}$, where v is the phonon group velocity and l is the phonon MFP. Therefore, Θ should drop to a value above zero at 0 K if phonon is the only heat carrier, and the value is correlated with defect-induced phonon MFP (l_0). Here, the single-relaxation-time approximation is only intended for basic physics explanation. The model in this work considers all of the phonon dispersion and various phonon branches in PE crystals[22,28,29,35] (see Supporting Information for more detailed description).

On the basis of the effective Θ_0 shown in Figure 6, which contains contribution from amorphous phase, l_0 values for unstretched UHMW-PE fibers are determined to be 7.35, 5.47, and 6.19 nm for samples A, B, and C, respectively. Through heat stretching, their l_0 increases up to 24.82, 14.95, and 13.63 nm. The l_0 calculated above is based on an assumption that the amorphous phase can be considered as defects in crystals or defective crystals. The other way is ruling out the contribution of amorphous phase to Θ. On the basis of a defined crystallinity and an assumption that the fiber sample is a homogenous composite of amorphous PE and crystal PE, the l_0 in crystalline phase can be evaluated. In the XRD characterization, the crystallinity of sample A is found to decrease from 92.09 to 82.54% through stretching. By applying effective medium approximation, the phonon MFP in sample A increases from 9.81 to 46.71 nm after stretching. The significantly elongated phonon MFP proposes a structural change inside the polymer, which favors phonon transport. This will be explained by the following structure characterization.

Raman spectroscopy (confocal Raman system; Voyage, B&W Tek, Inc.) is used to characterize the structural change along a stretched sample. The sample is a duplicate of sample

DOI: 10.1021/acsomega.7b00563
ACS Omega 2017, 2, 3931−3944

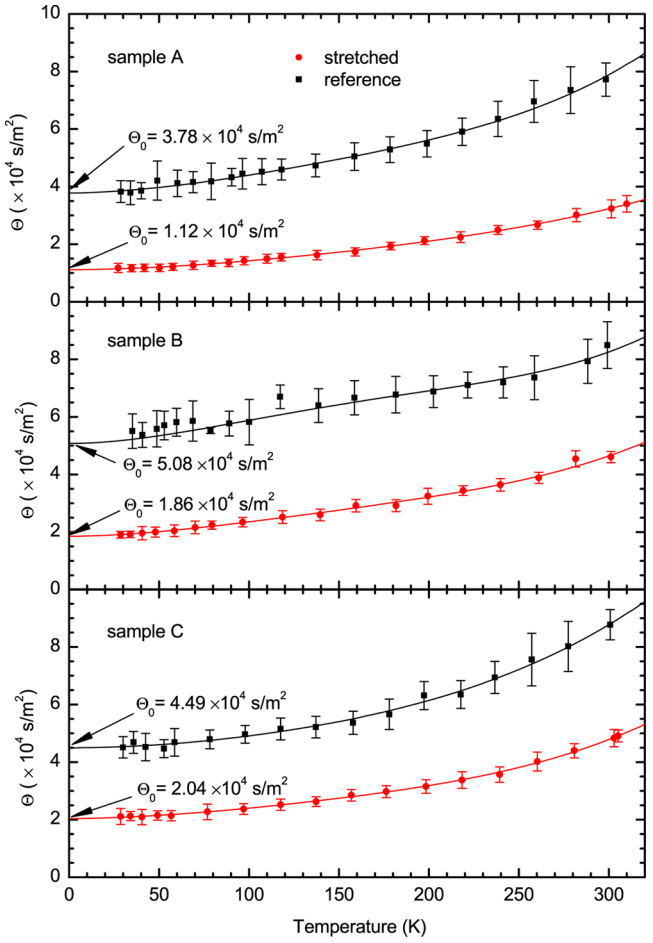

Figure 6. Θ vs temperature for samples A−C. Θ_0 is fitted from fourth-order polynomial regression. Each data point is a mean value of 20 repeated measurements. The error bar represents three standard deviations of the mean.

A. Laser beam (wavelength, 532 nm; laser power, 16 mW) scans from the center of heated region to the unheated region. The polarization of laser is perpendicular to the fiber axis. A series of Raman spectra are produced as shown in Figure 7a. The antisymmetric (1060 cm^{-1}) and symmetric (1130 cm^{-1}) C−C stretching bands represent vibration of skeletal chains parallel and perpendicular to the chain axis, respectively. The ratio of band area between the two bands does not change at different positions, which suggests consistent molecular alignment along a stretched fiber. The peak at 1296 cm^{-1} stands for CH_2 twisting mode. The sharp peak at 1416 cm^{-1} suggests the dominance of orthorhombic crystalline structure. The splitting peaks at 1440 and 1460 cm^{-1} stand for CH_2 bending vibration in interfacial (between amorphous phase and crystallites) amorphous chains and melt-like amorphous chains, respectively. Therefore, we can use the peak area ratio $A_{1296}/(A_{1440} + A_{1460})$ to evaluate crystallinity and A_{1440}/A_{1460} to evaluate the composition of the amorphous phase. Figure 7b shows insignificant variation of both peak area ratios. In Figure 7c, no obvious change in the full width at half-maximum (FWHM) is observed for the peaks at 1296, 1440, and 1460 cm^{-1}. This measurement is limited by the curved surface of fiber because the peak width and intensity could fluctuate when the laser spot on the surface slightly moves.

2.4. Crystallinity and Crystallite Size: Effect of Heat Stretching. *2.4.1. Crystallite Alignment.* For XRD characterization, 50 duplicates of sample A are aligned as a bundle and spread evenly in the form of a 30 mm × 1.5 mm thin film. Figure 8a,b shows the XRD pole-figure (Rigaku SmartLab diffractometer) patterns for the (002) plane of the stretched and reference fiber bundles. The two strong peaks at $\alpha = 0°$ and $\beta = 0/180°$ suggest that both samples are found highly oriented in the axial direction. Figure 8c is a schematic for the setup of XRD pole-figure measurement. For a more quantitative view, the diffraction intensity is integrated along α and the integrated intensity is plotted against the β angle in Figure 8d. We hardly find the difference of peak width between the stretched sample and its reference group. The FWHM values of intensity peaks are 10.4° at $\beta = 0$ and 8.02° at $\beta = 180°$ for the reference sample, and 10.5° at $\beta = 0$ and 7.1° at $\beta = 180°$ for stretched sample. The narrow width of pole-figure intensity peaks at $\beta = 0$ and 180° indicates that the sample fiber is highly oriented along the fiber axis no matter it is processed by heat stretching or not. Thus, all of these data entail negligible chain orientation change before and after stretching.

2.4.2. Crystallite Size. The XRD patterns (Bruker D8 Discover) for the fiber bundles are also given as shown in Figure 9. On the basis of the FHWM of the spectrum, the crystallite sizes for the stretched sample are determined to be 17.5 nm for (200) planes and 18.28 nm for the (002) plane. For the reference sample, the crystallite sizes are 17.4 and 18.34 nm for (200) and (002) planes, respectively. The negligible variation of crystallite size is contradicted to the defect-induced phonon MFP, which gets elongated to a great extent after heat stretching. It is potentially due to reduced scatterings at grain boundaries or enhanced phonon transport in amorphous regions sandwiched between crystallites. The reduced boundary scattering could result from decreased boundary roughness after heat stretching. It is because decreased roughness allows more specular phonon scatterings to replace diffuse scatterings at boundaries.[36] In the past, it has been proved that after heat stretching, the amorphous region will become more aligned along the drawing direction. Such alignment improvement will definitely enhance the phonon transmission from the crystalline region to the amorphous region, leading to an increased phonon MFP.

2.4.3. Crystallinity Reduction and Structure Physical Model. In addition, a new peak at the band of (010) plane is observed after heat stretching, which suggests that the monoclinic/triclinic crystals emerge and come to coexist with the dominant orthorhombic form. It is possible that the sample is cooled under tension. During cooling in air, the sample remains being suspended before reaching RT. The fiber could shrink during cooling, which therefore introduces stress. Orthorhombic PE crystals are found partially conformed to monoclinic/triclinic structures under stress.[37,38] The crystallinity, calculated by comparing the integrated area of crystalline peaks and amorphous peaks, decreases from 92.09 to 82.54% after stretching. The new peak has been considered in the fitting of peaks. The crystallinity of the original fiber agrees well with our previous measurement (91.9%).[22] However, the decreased crystallinity after stretching is definitely unexpected because it seems contrary to the k increase. We speculate that the observed significant increase in k is more induced by structure reconstructuring favorable for heat conduction.

On the basis of structural characterization results, the structure reconstructuring could happen in two ways. The first possible case is the relocation of amorphous structures. The nanocomposite model of UHMW-PE microfiber is used to

DOI: 10.1021/acsomega.7b00563
ACS Omega 2017, 2, 3931−3944

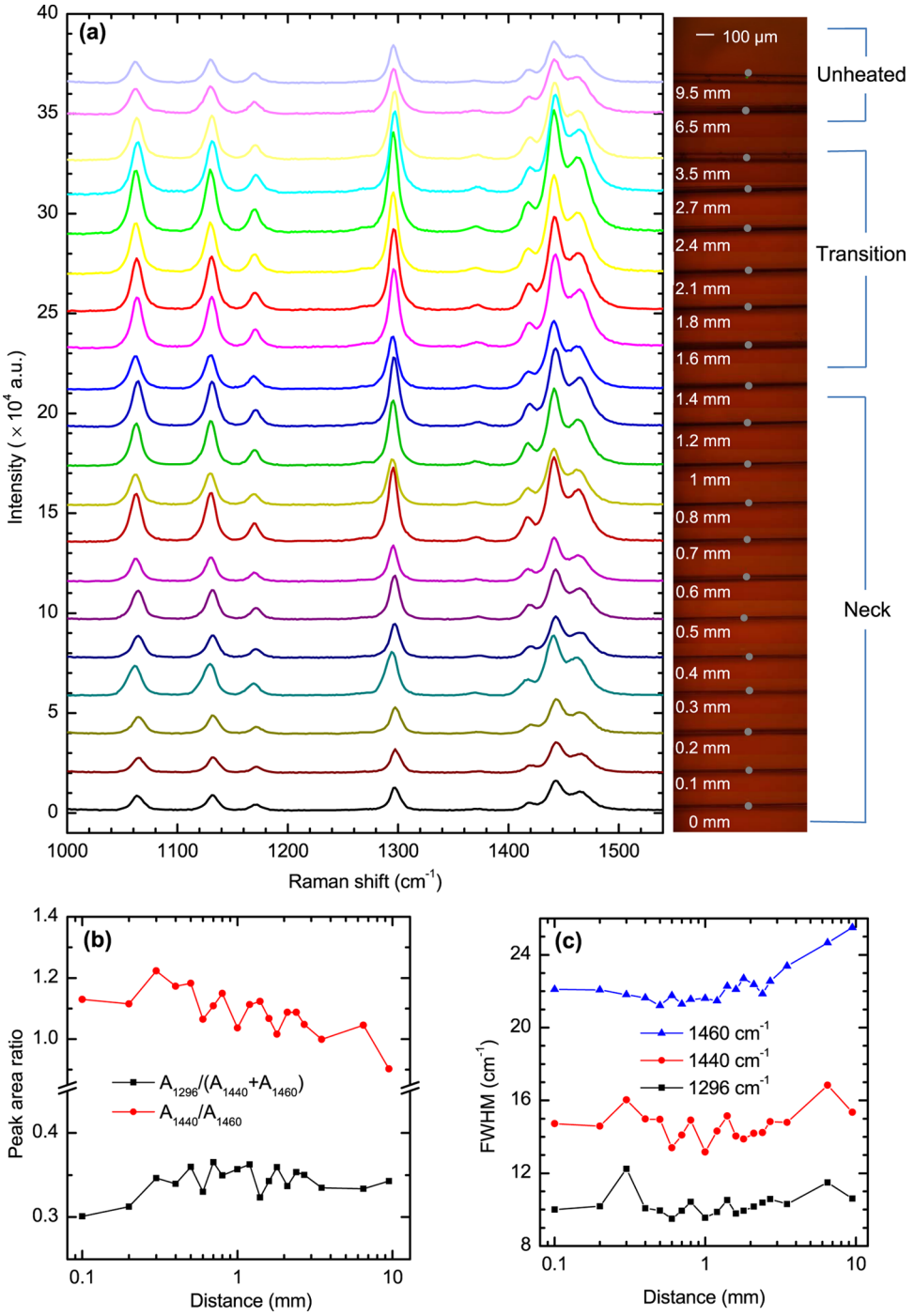

Figure 7. Raman spectroscopy for a stretched UHMW-PE fiber. (a) Raman spectra obtained at different positions along the sampled UHMW-PE fiber. The distance of the beam spot from the center of the neck region is presented on the right for each spectrum, with a microscope image. Beam spots are marked with gray spots. The integration time is 6 s for the unheated region and 10 s for the rest. (b) FWHM of peaks at 1296, 1440, and 1460 cm^{-1}. (c) Peak area ratios, including $A_{1296}/(A_{1440} + A_{1460})$ and A_{1440}/A_{1460}.

explain the effect of amorphous relocation. In the nanocomposite model, the UHMW-PE microfiber has a composite structure formed by aligned crystallites embedded in amorphous matrix, as shown in Figure 10a.[39] ϕ_c, $\phi_{a,\perp}$, and $\phi_{a,\parallel}$ are volumetric fractions of crystallites (white region), serially connected amorphous phase (blue region), and parallel connected amorphous phase (green region), respectively. Here, we assume that (1) the amorphous phase is homogeneous: $k_{a,\perp} = k_{a,\parallel} = k_a$ and (2) k_a and k_c remain unchanged during heat stretching. Then, the effective thermal conductivity (k_{eff}) in the fiber axis can be calculated on the basis of the thermal resistance network model, as shown in Figure 10b: $k_{eff} = (1 - \phi_{a,\parallel})^2 k_c k_a/(\phi_c k_a + \phi_{a,\perp} k_c) + \phi_{a,\parallel} k_a$. The XRD analysis gives $\phi_c \approx 92\%$ before stretching and $\phi_c \approx 83\%$ after stretching. To prove the existence of parallel connected amorphous phase, we propose that there is no amorphous structure connected in parallel with the crystalline structure. In other words, $\phi_{a,\parallel} = 0$ for the original PE fiber. Then, even if k_c and k_a are taken as the highest experimental values to our knowledge: $k_c = 100$ W/(m·K)[17] and $k_a = 0.3$ W/(m·K),[40] for original fibers, the calculated

DOI: 10.1021/acsomega.7b00563
ACS Omega 2017, 2, 3931−3944

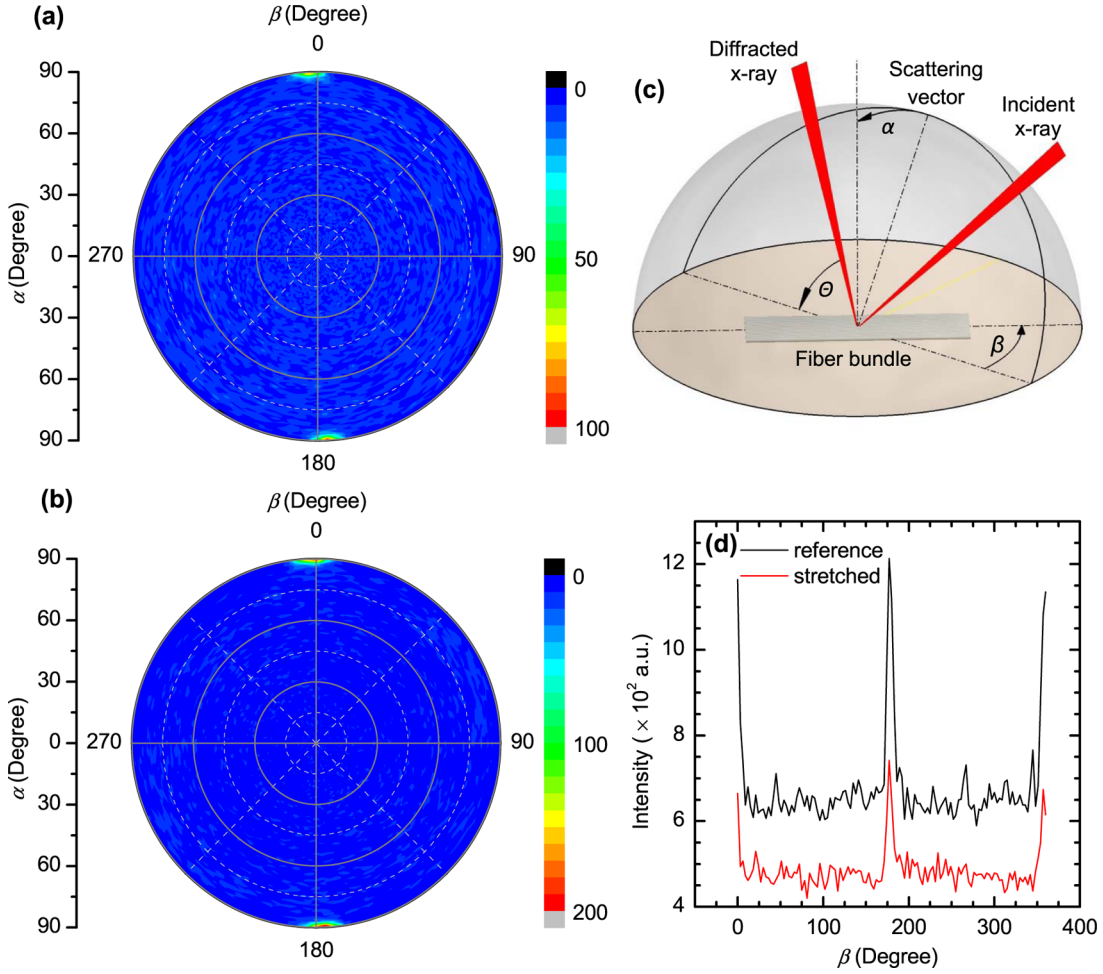

Figure 8. XRD patterns and intensity distributions of stretched and reference UHMW-PE fibers. (a) XRD pole figure for (002) plane of the stretched sample. (b) XRD pole figure for (002) of the reference sample. (c) Schematic of pole-figure XRD. (d) Intensity variation with varying β. The intensity for each β is an integrated value for α from 0 to 90°.

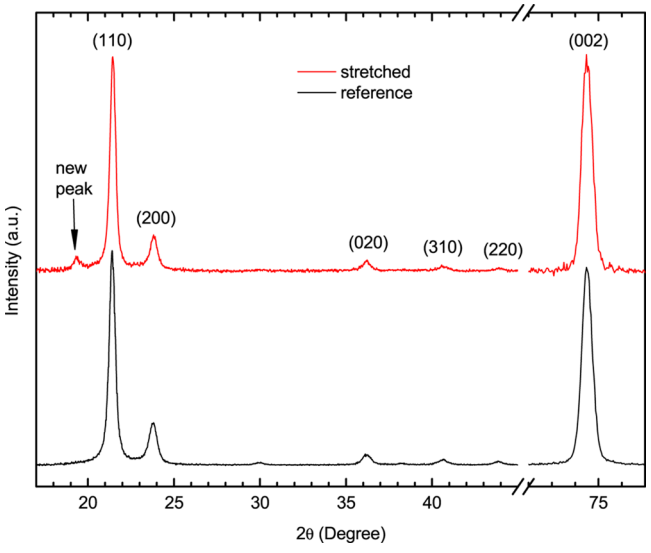

Figure 9. XRD pattern for the UHMW-PE fiber bundles. The patterns between 17 and 45° are obtained by an out-of-plane X-ray beam. The (002) peak around 75° is obtained by an in-plane X-ray beam.

value $k_{eff} \approx 3.6$ W/(m·K) is still fairly lower than the measured value, 21.3 W/(m·K). This contradiction denies the assumption that $\phi_{a,\parallel} = 0$, suggesting the existence of parallel connected amorphous region. Then, we can calculate $\phi_{a,\parallel}$ on the basis of the measured k value of sample A. Before stretching, $\phi_c \approx 92\%$ and $k_{eff} = 21.3$ W/(m·K). The $\phi_{a,\parallel}$ value is determined to be ~7.06% and $\phi_{a,\perp} \approx 0.94\%$. As for the stretched fibers given $\phi_c \approx 83\%$ and $k = 50.8$ W/(m·K), $\phi_{a,\parallel} \approx 16.84\%$ and $\phi_{a,\perp} \approx 0.16\%$. It is conclusive that k of the sampled UHMW-PE fibers is highly sensitive to the fraction of serially connected amorphous structure because nearly 140% k improvement is obtained when the serially connected amorphous fraction decreases by merely 0.78%. Sensitivity is presented in Figure 10c. As shown in the figure, if the serially connected amorphous fraction does not change, the crystallinity reduction by the stretching will give a slight decrease of k. However, a small decrease in $\phi_{a,\perp}$ will increase k significantly.

This first case could be supported by a bending test. A stretched fiber and an original fiber are bent by hand repeatedly. The stretched fiber used in the test is stretched under the same condition as sample A. The performance of the bending test is recorded as a video in Supporting Information. The test shows that a rugged surface appears on the stretched fiber after repeated bending, whereas the original fiber still has a smooth and aligned surface as before bending (Figure 11). The rugged surface suggests the occurrence of plastic deformation in the bent region. The UHMW-PE fiber could lose some

DOI: 10.1021/acsomega.7b00563
ACS Omega 2017, 2, 3931−3944

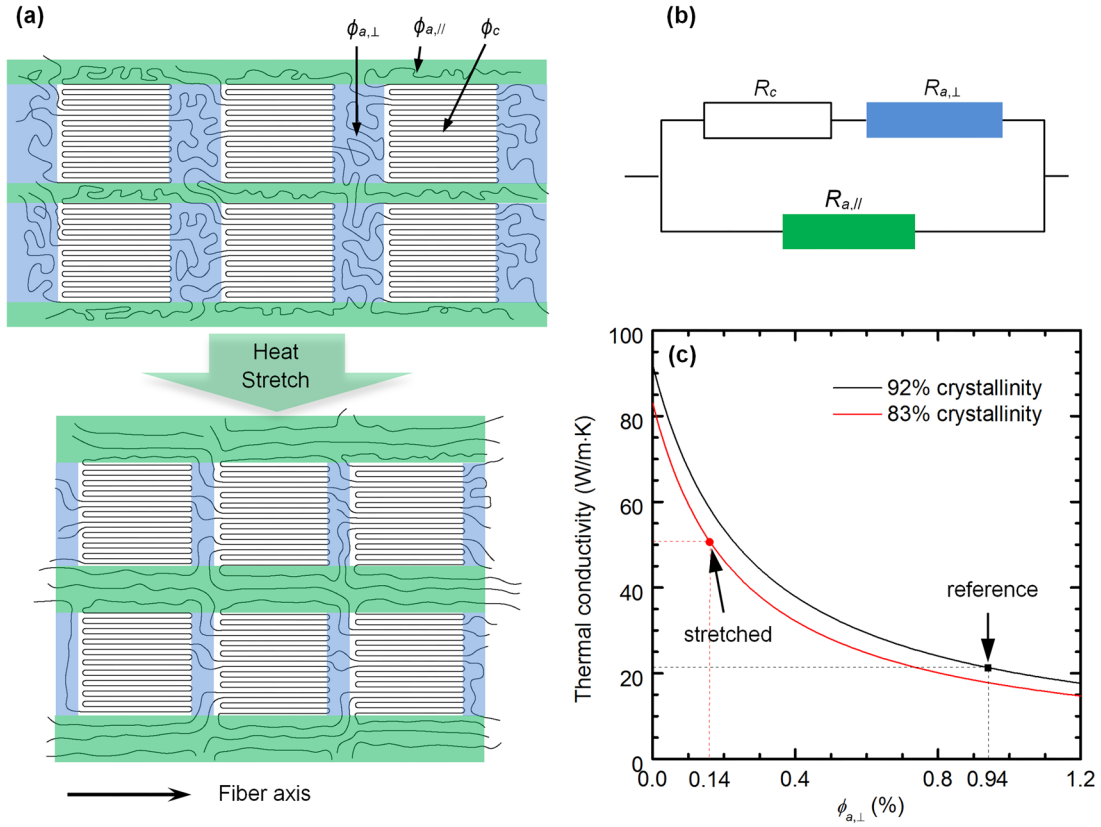

Figure 10. Proposed physics model: (a) Structural model of UHMW-PE fiber before and after heat stretching, with fiber axis in the horizontal direction. The volumetric fractions are denoted by $\phi_{a,\perp}$, $\phi_{a,\|}$, and ϕ_c for serial amorphous regions, parallel amorphous regions, and crystalline regions, respectively. (b) Thermal resistance network model for thermal transport along fiber axis. $R_{a,\perp}$, $R_{a,\|}$, and R_c are the thermal resistances of serial amorphous region, parallel amorphous region, and crystalline region, respectively. For a sample of unit length and unit cross-sectional area, $R_{a,\perp} = \phi_{a,\perp}/[k_a(\phi_{a,\perp} + \phi_c)^2]$, $R_{a,\|} = 1/k_a\phi_{a,\|}$, $R_c = \phi_c/[k_a(\phi_{a,\perp} + \phi_c)^2]$, and $1/R_{eff} = 1/R_{a,\|} + 1/(R_{a,\perp} + R_c)$. (c) Thermal conductivity variation against the fraction of serially connected amorphous region. The data points for reference and stretched samples are determined by the k measured by the TET technique and the crystallinities given by XRD analysis.

elasticity during heat stretching, potentially resulted from the reduced fraction of serially connected amorphous structure. For instance, if there is no serially connected amorphous structure, the crystalline part could be more easily bent to have plastic change or to break.

The second possible case is the improved alignment of amorphous phase. It has been documented that the amorphous structure could be partially aligned to the stretching direction during mechanical stretching.[41,42] If the k of amorphous structures is enhanced due to the alignment of amorphous chains, then the overall k will be able to increase even when crystalline fraction decreases. To study the orientation of amorphous structures in samples, polarized Raman spectroscopy is employed here by adding a polarizer to the confocal Raman system. A laser beam is focused on the neck region of a sample stretched under the same condition as sample A. As introduced in the literature,[43] the intensity of crystalline bands at 1296 and 1416 cm^{-1} becomes higher as laser polarization is gradually aligned to the c-axis of PE crystallites from a perpendicular position ($\gamma = 90°$). It is reasonable to assume that c-axis of PE crystallite is parallel to the fiber axis (or stretching direction) here based on the XRD analysis. A reverse trend is found for the amorphous bands at 1440 and 1460 cm^{-1}. These phenomena also occur in our sample, as shown in Figure 12a. Only the spectra of the stretched fiber are presented here because those of the reference sample share the same trend as polarization varies. Therefore, the change of the relative intensity of polarized Raman spectra could be used to indicate the degree of orientation. Figure 12b,c shows the variation of relative intensities with varying angle between polarization and fiber axis (γ) for reference and stretched samples, respectively. As seen, by comparing the percentage intensity variation along γ, obviously enhanced anisotropy in amorphous region and slightly reduced anisotropy for crystallites can be found. For example, the relative intensity of 1296 cm^{-1} band drops by ~60% before stretching and by ~50% after stretching when γ is changed from 0 to 90°, indicating a reduced structural anisotropy for crystal PE. However, this slight alignment reduction cannot be revealed in our pole-figure analysis using XRD. Then, we compare the intensities of the four peaks at a certain γ. As $\gamma = 0°$, the relative intensities of amorphous peaks remain unchanged before and after stretching although the amorphous fraction increases after stretching, according to XRD analysis. This proposes a reduced fraction of unaligned amorphous structures in the amorphous region because the crystalline fraction decreases after stretching. As $\gamma = 90°$, stronger bands for parallel amorphous structure and perpendicular crystallites alignment are found. It indicates that unaligned crystallites and aligned amorphous structure increase in quantity after stretching. As we indicated above, the reduction in the alignment in the crystalline structure is rather trivial. However, the alignment improvement in the amorphous

DOI: 10.1021/acsomega.7b00563
ACS Omega 2017, 2, 3931−3944

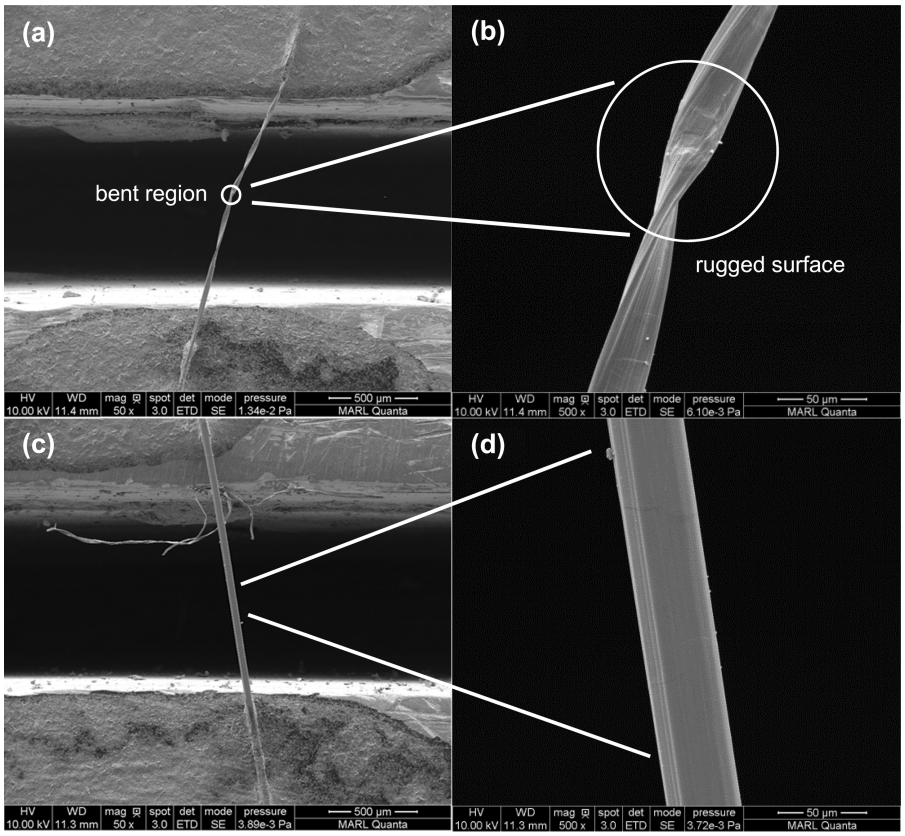

Figure 11. SEM images of the UHMW-PE fibers after repeated bending. (a) A sample that is stretched under the same condition as sample A and bent for several times. The bent part locates in the middle of the gap. (b) The surface of the bent part of the sample in (a). The surface turns from a smooth and aligned shape to a rugged shape, indicating the occurrence of irreversible deformation during bending. (c) An original sample after being bent repeatedly. (d) The bent part of the original sample. It is hard to find from the SEM image where it is bent. The bending test indicates that the UHMW-PE loses some elasticity during heat stretching, potentially resulted from the reduced fraction of serially connected amorphous structure.

structure is more obvious. After stretching, the anisotropic ratio of CH_2 bending vibration near 1440 and 1460 cm^{-1} have an intensity increase of 536 and 348%, respectively, when γ changes from 0 to 90°. Before stretching, this increase is only 372 and 257%, respectively. The amplified anisotropic nature of bending vibration in amorphous chains suggests that amorphous chains are more aligned to the fiber axis, which can lead to a substantial enhancement in k. In conclusion, the polarized Raman study shows that the amorphous chains turn to be more aligned although some crystallites become less aligned. The high k (~350) of a single PE molecular chain suggests a great potential for k enhancement by aligning carbon chains. It allows more heat load be transferred by the backbones of PE in the same direction. This will significantly reduce the huge thermal resistance of the amorphous structure among crystallites in the axis direction, leading to a great k enhancement in overall.

Besides the two assumptions based on experimental evidence, there is a third case, which is possible but not covered by the experimental study in this work. It must be remembered that the stretching process ends with quenching in ambient air. The cooling process could end in 1−2 s in the case of sample A. During cooling, a temperature gradient should exist along the fiber, with the highest temperature in the center. The temperature gradient can guide the orientation of growing crystalline lamellae. However, the recrystallization could be stopped on its half way, which makes the crystal melts stay amorphous in terms of XRD analysis. The partial melting of crystalline phase allows the chain movement, which functions together with the temperature gradient to make an overall improved alignment. The increased amorphous fraction should come from the molten crystals, which might sustain better heat conduction but not be detectable by XRD.

3. CONCLUSIONS

In summary, we have made breakthrough advance in increasing the k of crystalline UHMW-PE microfibers from 19−22 W/(m·K) (unstretched) to a value of 50.8 W/(m·K), representing the highest repeatable and engineering level k increase for PE microfibers. The highest k is obtained when the UHMW-PE fiber is stretched at a temperature (131.5 °C) near the melting point with a low strain rate (0.0129 s^{-1}) and a low final strain ratio (~6.6). Furthermore, we discovered that the amorphous structure fraction increases after stretching, but such more amorphous-composed material rather sustains a much higher k than the highly aligned original sample of higher crystal fraction. A general trend of higher k with higher stretching temperature is observed. k drops when the stretching temperature increases very close to the melting point (~135 °C), likely due to the absence of stress when crystallites melt. Calculations based on thermal reffusivity at the 0 K limit showed that the defect-induced phonon MFP increases significantly after heat stretching. XRD pole-figure analysis provided evidence that the orientation of crystallites barely changes after stretching, which points physics reasons to the amorphous region for significant k increase. Polarized Raman

DOI: 10.1021/acsomega.7b00563
ACS Omega 2017, 2, 3931−3944

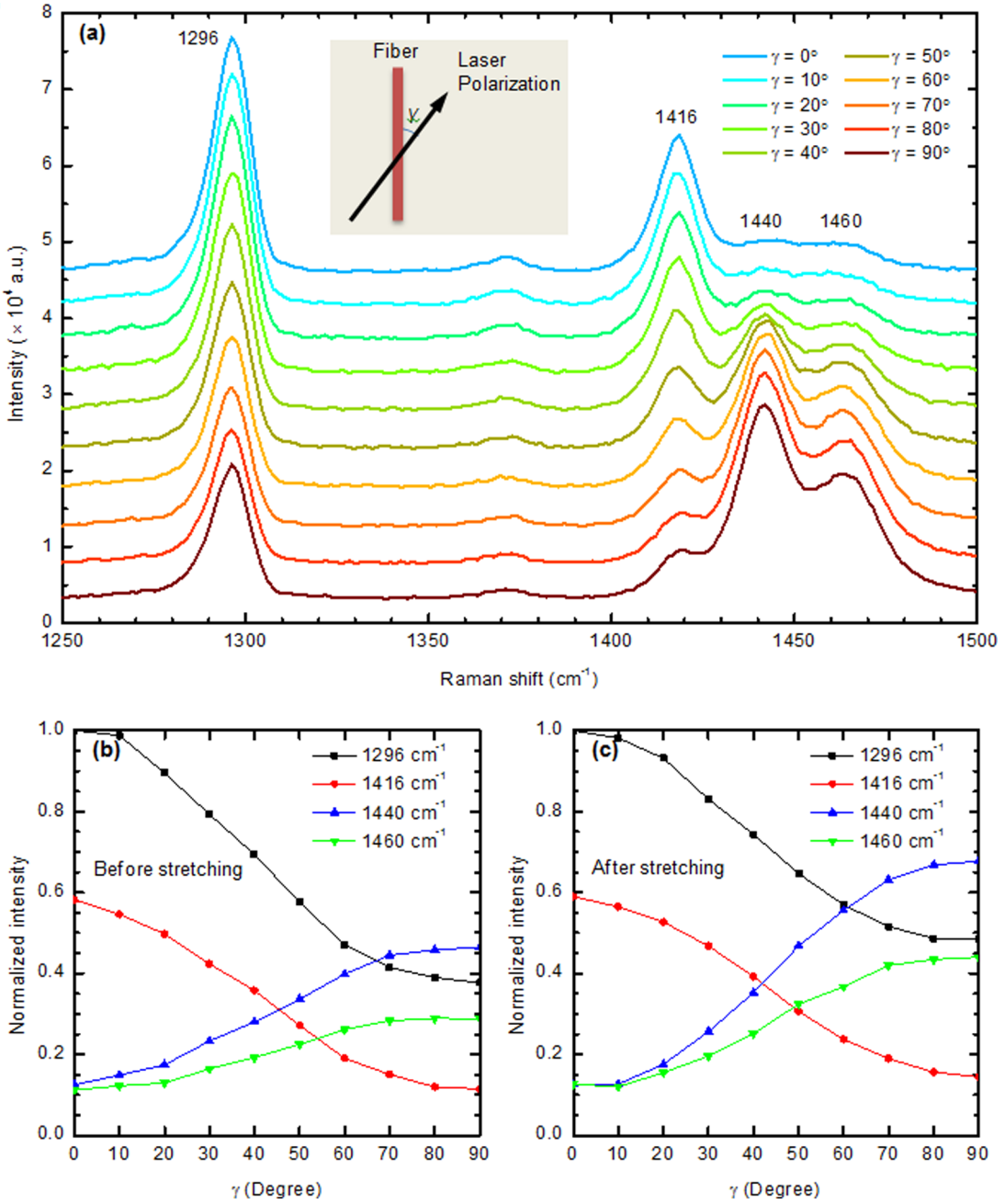

Figure 12. Polarized Raman spectroscopy for an UHMW-PE microfiber before and after stretching: (a) Raman spectra of stretched fiber sample with varied γ, where γ is the angle between fiber axis and laser polarization. (b, c) Normalized peak intensity vs γ for the sample before and after stretching, respectively. The peak intensities have been normalized by the intensity at 1296 cm^{-1} when the polarization is parallel to fiber axis (γ = 0°).

spectroscopy indicates that the amorphous structure became more aligned after stretching. Aligned amorphous chains lead to enhanced thermal conductivity in the amorphous region, which can significantly increase the overall thermal conductivity. Our bending test of the stretched samples shows more plasticity, suggesting a reduced fraction of amorphous structure among crystallites previously existing in the fiber axial direction. Even this small amount of reduction in the serially connected amorphous structure will increase the overall thermal conductivity significantly.

■ ASSOCIATED CONTENT

Supporting Information

The Supporting Information is available free of charge on the ACS Publications website at DOI: 10.1021/acsomega.7b00563.

Heat stretching, TET technique, thermal reffusivity and defect-induced phonon MFP, differential scanning calorimeter analysis of original S-900 fiber (PDF)

Two videos showing the performance of the bending test for a stretched fiber and an original fiber (MPG) (MPG)

DOI: 10.1021/acsomega.7b00563
ACS Omega 2017, 2, 3931−3944

AUTHOR INFORMATION

Corresponding Authors

*E-mail: shxu16@sues.edu.cn. Tel: 001-86-138-164-26219 (S.X.).
*E-mail: xwang3@iastate.edu. Tel: 001-515-294-8023 (X.W.).

ORCID

Xinwei Wang: 0000-0002-9373-3750

Author Contributions

X.W., S.X., and B.Z. conceived and designed the experiments. B.Z. and J.L. performed the experiments. B.Z., S.X., and X.W. conducted data analysis. S.V. contributed to XRD and pole-figure XRD analysis. T.W. conducted polarized Raman analysis. M.H. conducted differential scanning calorimeter analysis. J.L. conducted phonon scattering analysis.

Notes

The authors declare no competing financial interest.

ACKNOWLEDGMENTS

National Science Foundation (CBET1235852, CMMI1264399), Department of Energy (DENE0000671, DE-EE0007686), and Iowa Energy Center (MG-16-025, OG-17-005) are gratefully acknowledged for supporting this work. The authors are grateful to Minifibers, Inc. for providing the Spectra S-900 samples used in this work.

REFERENCES

(1) Brinson, H. F.; Brinson, L.C. Characteristics, Applications and Properties of Polymers. In *Polymer Engineering Science and Viscoelasticity: An Introduction*; Springer US: Boston, MA, 2008; pp 55−97.

(2) Laaber, D.; Bart, H.-J. Chemical Resistance and Mechanical Stability of Polymer Film Heat Exchangers. *Chem. Ing. Tech.* **2015**, *87*, 306−311.

(3) Neikirk, C. C.; Chung, J. W.; Priestley, R. D. Modification of mechanical properties in polymer nanocomposites by the incorporation of specific self-complementary hydrogen bonding interactions. *Polymer* **2015**, *79*, 212−220.

(4) Sperling, L. H. *Introduction to Physical Polymer Science*, 4th ed.; John Wiley & Sons: Hoboken, NJ, 2006.

(5) Choy, C. L. Thermal conductivity of polymers. *Polymer* **1977**, *18*, 984−1004.

(6) Santos, W. N. D.; Gregorio, R. Hot-wire parallel technique: A new method for simultaneous determination of thermal properties of polymers. *J. Appl. Polym. Sci.* **2002**, *85*, 1779−1786.

(7) Washo, B. D.; Hansen, D. Heat Conduction in Linear Amorphous High Polymers: Orientation Anisotropy. *J. Appl. Phys.* **1969**, *40*, 2423−2427.

(8) Morelli, D. T.; Heremans, J.; Sakamoto, M.; Uher, C. Anisotropic Heat Conduction in Diacetylenes. *Phys. Rev. Lett.* **1986**, *57*, 869−872.

(9) Piraux, L.; Kinany-Alaoui, M.; Issi, J.-P.; Begin, D.; Billaud, D. Thermal conductivity of an oriented polyacetylene film. *Solid State Commun.* **1989**, *70*, 427−429.

(10) Choy, C.; Wong, Y.; Yang, G.; Kanamoto, T. Elastic modulus and thermal conductivity of ultradrawn polyethylene. *J. Polym. Sci., Part B: Polym. Phys.* **1999**, *37*, 3359−3367.

(11) Kurabayashi, K. Anisotropic Thermal Properties of Solid Polymers. *Int. J. Thermophys.* **2001**, *22*, 277−288.

(12) Hung, M. T. Heat Transport in Polymer Thin Films for Micro/Nano-Manufacturing. Ph.D. Dissertation, University of California, 2007.

(13) Liu, J.; Yang, R. Tuning the thermal conductivity of polymers with mechanical strains. *Phys. Rev. B: Condens. Matter Mater. Phys.* **2010**, *81*, No. 174122.

(14) Fujishiro, H.; Ikebe, M.; Kashima, T.; Yamanaka, A. Thermal conductivity and diffusivity of high-strength polymer fibers. *Jpn. J. Appl. Phys.* **1997**, *36*, 5633.

(15) Wang, X.; Ho, V.; Segalman, R. A.; Cahill, D. G. Thermal Conductivity of High-Modulus Polymer Fibers. *Macromolecules* **2013**, *46*, 4937−4943.

(16) Ma, J.; Zhang, Q.; Mayo, A.; Ni, Z.; Yi, H.; Chen, Y.; Mu, R.; Bellan, L. M.; Li, D. Thermal conductivity of electrospun polyethylene nanofibers. *Nanoscale* **2015**, *7*, 16899−16908.

(17) Shen, S.; Henry, A.; Tong, J.; Zheng, R.; Chen, G. Polyethylene nanofibres with very high thermal conductivities. *Nat. Nanotechnol.* **2010**, *5*, 251−255.

(18) Henry, A.; Chen, G. High thermal conductivity of single polyethylene chains using molecular dynamics simulations. *Phys. Rev. Lett.* **2008**, *101*, No. 235502.

(19) Kanamoto, T.; Tsuruta, A.; Tanaka, K.; Takeda, M.; Porter, R. S. Super-drawing of ultrahigh molecular weight polyethylene. 1. Effect of techniques on drawing of single crystal mats. *Macromolecules* **1988**, *21*, 470−477.

(20) Choy, C.; Leung, W.; Ng, Y. Thermal diffusivity of polymer films by the flash radiometry method. *J. Polym. Sci., Part B: Polym. Phys.* **1987**, *25*, 1779−1799.

(21) Shi, L. Mesoscopic Thermophysical Measurements of Microstructures and Carbon Nanotubes. Ph.D. Dissertation, University of California, 2001.

(22) Liu, J.; Xu, Z.; Cheng, Z.; Xu, S.; Wang, X. Thermal Conductivity of Ultrahigh Molecular Weight Polyethylene Crystal: Defect Effect Uncovered by 0 K Limit Phonon Diffusion. *ACS Appl. Mater. Interfaces* **2015**, *7*, 27279−27288.

(23) Rudy, C. W.; Marandi, A.; Vodopyanov, K. L.; Byer, R. L. In-situ Tapering of Chalcogenide Fiber for Mid-infrared Supercontinuum Generation. *J. Visualized Exp.* **2013**, No. e50518.

(24) Guo, J.; Wang, X.; Wang, T. Thermal characterization of microscale conductive and nonconductive wires using transient electrothermal technique. *J. Appl. Phys.* **2007**, *101*, No. 063537.

(25) Lin, H.; Xu, S.; Wang, X.; Mei, N. Thermal and Electrical Conduction in Ultrathin Metallic Films: 7 nm down to Sub-Nanometer Thickness. *Small* **2013**, *9*, 2585−2594.

(26) Bourgeois, O.; Fournier, T.; Chaussy, J. Measurement of the thermal conductance of silicon nanowires at low temperature. *J. Appl. Phys.* **2007**, *101*, No. 016104.

(27) Li, D.; Wu, Y.; Kim, P.; Shi, L.; Yang, P.; Majumdar, A. Thermal conductivity of individual silicon nanowires. *Appl. Phys. Lett.* **2003**, *83*, 2934−2936.

(28) Henry, A.; Chen, G. High thermal conductivity of single polyethylene chains using molecular dynamics simulations. *Phys. Rev. Lett.* **2008**, *101*, No. 235502.

(29) Chang, S. Heat-capacities of polyethylene from 2 to 360 K. 2. 2 High-density linear polyethylene samples and thermodynamic properties of crystalline linear polyethylene. *J. Res. Natl. Bur. Stand., Sect. A* **1974**, *78A*, 387−400.

(30) Smith, P.; Lemstra, P. J.; Pijpers, J. P. L.; Kiel, A. M. Ultra-drawing of high molecular weight polyethylene cast from solution. *Colloid Polym. Sci.* **1981**, *259*, 1070−1080.

(31) Smith, P.; Chanzy, H. D.; Rotzinger, B. P. Drawing of virgin ultrahigh molecular weight polyethylene: An alternative route to high strength/high modulus materials. *J. Mater. Sci.* **1987**, *22*, 523−531.

(32) Yeh, J.-T.; Lin, S.-C.; Tu, C.-W.; Hsie, K.-H.; Chang, F.-C. Investigation of the drawing mechanism of UHMWPE fibers. *J. Mater. Sci.* **2008**, *43*, 4892−4900.

(33) Choy, C. L.; Luk, W. H.; Chen, F. C. Thermal conductivity of highly oriented polyethylene. *Polymer* **1978**, *19*, 155−162.

(34) Xu, Z.; Wang, X.; Xie, H. Promoted electron transport and sustained phonon transport by DNA down to 10 K. *Polymer* **2014**, *55*, 6373−6380.

(35) Stuart, S. J.; Tutein, A. B.; Harrison, J. A. A reactive potential for hydrocarbons with intermolecular interactions. *J. Chem. Phys.* **2000**, *112*, 6472−6486.

DOI: 10.1021/acsomega.7b00563
ACS Omega 2017, 2, 3931−3944

(36) Ziman, J. M. *Electrons and Phonons: the Theory of Transport Phenomena in Solids*; Oxford University Press: New York, 1960.
(37) Hsieh, Y. L.; Hu, X. P. Structural transformation of ultra-high modulus and molecular weight polyethylene fibers by high-temperature wide-angle X-ray diffraction. *J. Polym. Sci., Part B: Polym. Phys.* **1997**, *35*, 623−630.
(38) Fagnano, C.; Rossi, M.; Porter, R. S.; Ottani, S. A study on solid-state drawn fibers of polyethylene by confocal Raman microspectrometry: evaluation of the orientation profiles of amorphous and crystalline phases across the fiber section. *Polymer* **2001**, *42*, 5871−5883.
(39) Kavesh, S.; Prevorsek, D. C. Ultra High Strength, High Modulus Polyethylene Spectra Fibers and Composites. *Int. J. Polym. Mater. Polym. Biomater.* **1995**, *30*, 15−56.
(40) Kalaprasad, G.; Pradeep, P.; Mathew, G.; Pavithran, C.; Thomas, S. Thermal conductivity and thermal diffusivity analyses of low-density polyethylene composites reinforced with sisal, glass and intimately mixed sisal/glass fibres. *Compos. Sci. Technol.* **2000**, *60*, 2967−2977.
(41) Stein, N. The x-ray diffraction, birefringence, and infrared dichroism of stretched polyethylene. *J. Polym. Sci.* **1956**, *21*, 381−396.
(42) Holmes, D. R.; Palmer, R. P. The orientation of the crystalline and amorphous regions in polyethylene film. *J. Polym. Sci.* **1958**, *31*, 345−358.
(43) Takahashi, Y.; Puppulin, L.; Zhu, W.; Pezzotti, G. Raman tensor analysis of ultra-high molecular weight polyethylene and its application to study retrieved hip joint components. *Acta Biomater.* **2010**, *6*, 3583−3594.

DOI: 10.1021/acsomega.7b00563
ACS Omega 2017, 2, 3931−3944